

7-1-2005

On the Validity of the Parabolic Effective-Mass Approximation for the I-V Calculation of Silicon Nanowire Transistors

Jim Wang

Purdue University - Main Campus

Anisur Rahman

Purdue University - Main Campus

Avik Ghosh

Purdue University - Main Campus

Gerhard Klimeck

Purdue University - Main Campus, gekco@purdue.edu

Mark Lundstrom

Purdue University - Main Campus

Follow this and additional works at: <http://docs.lib.purdue.edu/nanodocs>

Wang, Jim; Rahman, Anisur; Ghosh, Avik; Klimeck, Gerhard; and Lundstrom, Mark, "On the Validity of the Parabolic Effective-Mass Approximation for the I-V Calculation of Silicon Nanowire Transistors" (2005). *Other Nanotechnology Publications*. Paper 118.
<http://docs.lib.purdue.edu/nanodocs/118>

This document has been made available through Purdue e-Pubs, a service of the Purdue University Libraries. Please contact epubs@purdue.edu for additional information.

On the Validity of the Parabolic Effective-Mass Approximation for the I – V Calculation of Silicon Nanowire Transistors

Jing Wang, *Student Member, IEEE*, Anisur Rahman, Avik Ghosh, Gerhard Klimeck, *Member, IEEE*, and Mark Lundstrom, *Fellow, IEEE*

Abstract—This paper examines the validity of the widely used parabolic effective-mass approximation for computing the current–voltage (I – V) characteristics of silicon nanowire transistors (SNWTs). The energy dispersion relations for unrelaxed Si nanowires are first computed by using an $sp^3d^5s^*$ tight-binding (TB) model. A seminumerical ballistic field-effect transistor model is then adopted to evaluate the I – V characteristics of the (n-type) SNWTs based on both a TB dispersion relation and parabolic energy bands. In comparison with the TB approach, the parabolic effective-mass model with bulk effective-masses significantly overestimates SNWT threshold voltages when the wire width is <3 nm, and ON-currents when the wire width is <5 nm. By introducing two analytical equations with two tuning parameters, however, the effective-mass approximation can well reproduce the TB I – V results even at a ~ 1.36 -nm wire width.

Index Terms—Bandstructure, effective-mass, field-effect transistor (FET), nanowire, nonparabolicity, quantum confinement, tight binding.

I. INTRODUCTION

AS MOSFET gate lengths enter the sub-50-nm regime, short-channel effects become increasingly severe [1]. To further scale down MOSFETs, device structures with new gate configurations are preferred to provide better electrostatic control than planar structures. For this reason, silicon nanowire transistors (SNWTs), which allow multigate or gate-all-around structures, are being extensively explored by different experimental groups [2]–[5]. Rapid experimental progress in SNWTs has shown their potential applications in future electronics.

To understand the device physics of SNWTs and to assess their performance limits, simulation work is important. Recently, three-dimensional quantum mechanical simulations of (n-type) SNWTs [or Fin field-effect transistors (FETs)] have been accomplished based on the parabolic effective-mass approximation [6]–[8]. Due to the two-dimensional quantum confinement, however, the bulk crystal symmetry is not preserved in Si nanowires. For this reason, quantitative results obtained from the parabolic effective-mass approximation are expected to suffer errors when the nanowire diameter is small. In this paper, we explore the validity of the parabolic

Manuscript received December 8, 2004; revised April 18, 2005. This work was supported by the Semiconductor Research Corporation (SRC), and the NSF Network for Computational Nanotechnology (NCN) under Grant EEC-0228390. The review of this paper was arranged by Editor R. Singh.

The authors are with the School of Electrical and Computer Engineering, Purdue University, West Lafayette, IN 47907 USA (e-mail: jingw@purdue.edu).
Digital Object Identifier 10.1109/TED.2005.850945

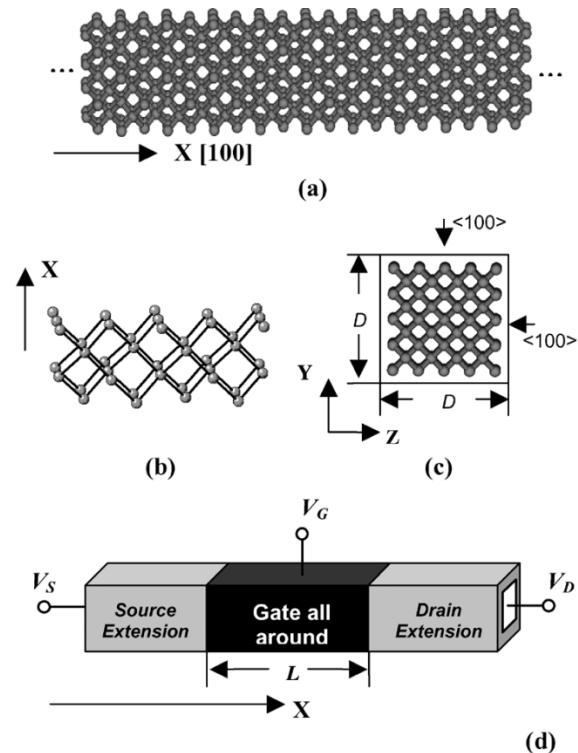


Fig. 1. (a) Atomic structure of a square nanowire ($D = 1.36$ nm) with a [100] transport direction. (b) A unit cell of the square nanowire illustrated in (a). (c) The schematic diagram of the cross section of the square nanowire. D denotes the edge length of the square cross section and the four faces of the square are all along the equivalent $\langle 100 \rangle$ axes. (d) A schematic diagram of the simulated gate-all-around nanowire transistors.

effective-mass approximation for the current–voltage (I – V) calculation of silicon nanowire transistors. We first compute the energy dispersion (E – k) relations of Si nanowires by a semiempirical $sp^3d^5s^*$ nearest-neighbor tight-binding (TB) approach [9]–[12]. The I – V characteristics of n-type SNWTs are then evaluated by a seminumerical ballistic FET model [13]–[15] using both the tight-binding E – k relations and parabolic energy bands. By comparing the results for the two types of E – k relations, the validity of the parabolic effective-mass approximation is examined.

This paper is divided into the following sections. Section II describes the $sp^3d^5s^*$ TB approach and illustrates the calculated atomistic nanowire bandstructures. In Section III, we first examine the validity of the parabolic effective-mass approximation for n-type SNWT simulations and then propose a tuning

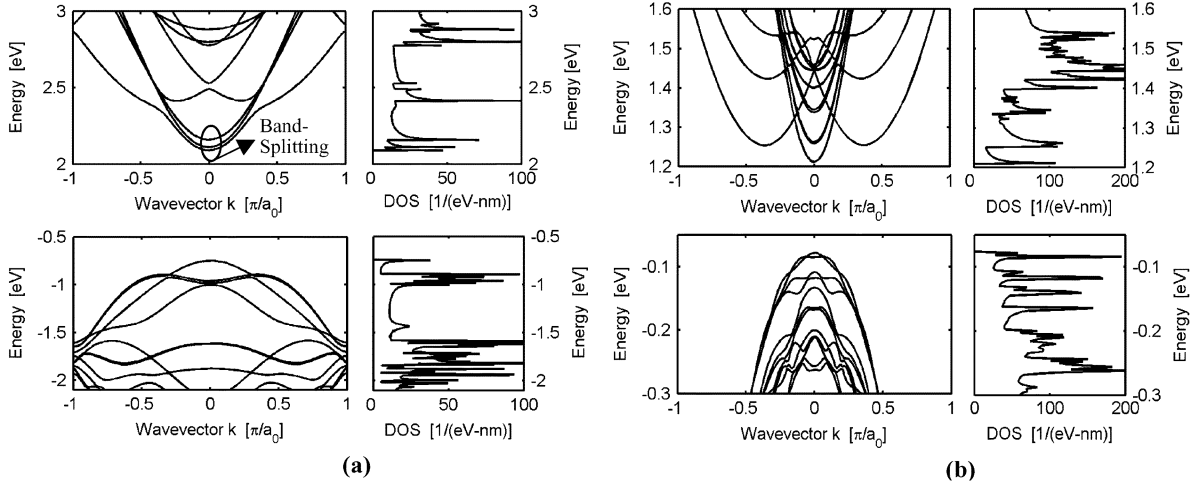


Fig. 2. Tight-binding E - k relations and the corresponding density-of-states (DOS) for the simulated Si nanowire structures with (a) $D = 1.36$ nm and (b) $D = 5.15$ nm. The conduction band for the thinner wire ($D = 1.36$ nm) displays significant band splitting at the Γ point.

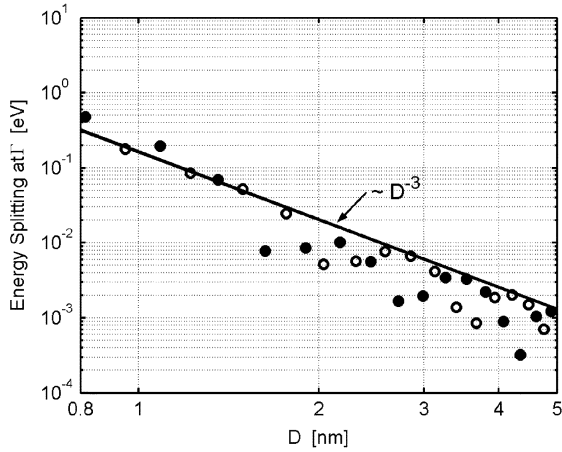


Fig. 3. Splitting energy (at the Γ point) versus wire width (D) for the simulated Si nanowires. The closed circles are for the wires with an odd number of atomic layers while the open circles are for the ones with an even number of atomic layers. The splitting energy fluctuates with D and the envelope decreases according to $\sim D^{-3}$.

procedure to modify the effective-mass approach for a better agreement with the TB calculation. Section IV summarizes key findings of this paper.

II. TB CALCULATION OF BANDSTRUCTURES

Fig. 1 shows an example of the simulated nanowire structures in this paper. The transport orientation of the wire is along the [100] direction [see Fig. 1(a)], the shape of the cross section is square, and the faces of the square are all along the equivalent $\langle 100 \rangle$ axes [see Fig. 1(c)]. Fig. 1(b) illustrates a unit cell of the nanowire crystal, which consists of four atomic layers along the x (transport) direction and has a length of $a_0 = 5.43 \text{ \AA}$. It should be noted that although Fig. 1 is only for a nanowire with a wire width $D = 1.36$ nm, nanowires with various wire widths (from 1.36 to 6.79 nm) are explored in this paper.

According to the TB approach adopted in this paper, 20 orbitals, consisting of an $sp^3d^5s^*$ basis with spin-orbital coupling, are used to represent each atom in the nanowire Hamiltonian. The orbital-coupling parameters we use are from [9], which have been optimized by Boykin *et al.* to accurately reproduce

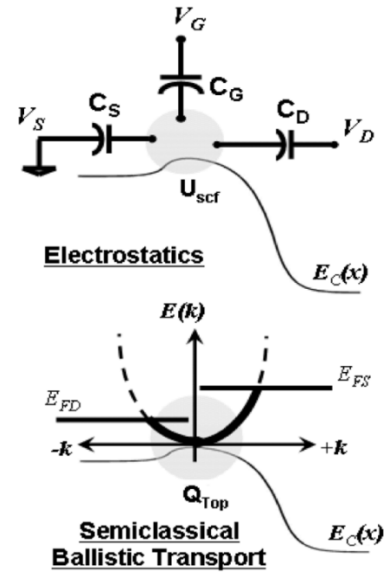


Fig. 4. Illustration of the essential aspects of the seminumerical ballistic FET model. The $E_C(x)$ curve represents the lowest electron subband in the device.

the bandgap and effective-masses of bulk Si (within a $<5\%$ deviation from the target values [9]). (It should be mentioned that bulk bond lengths are assumed in this paper. In real nanowires, the crystal structures will relax to obtain a minimum energy [16]. We expect that the general results of this study will also apply to relaxed structures while some quantitative differences may appear.) At the Si surfaces, a hard wall boundary condition for the wavefunction is applied and the dangling bonds at these surfaces are passivated using a hydrogen-like termination model of the sp^3 hybridized interface atoms. As demonstrated in [17], this technique successfully removes all the surface states from the semiconductor band gap.

Fig. 2 shows the E - k relations (left column) and the corresponding density-of-states (right column) for the simulated Si nanowires with wire widths (a) $D = 1.36$ nm and (b) $D = 5.15$ nm. It is clear that the six equivalent Δ valleys in the bulk Si conduction band split up into two groups due to quantum confinement. Four unprimed valleys, [010], [0 $\bar{1}$ 0], [001], and [00 $\bar{1}$], are projected to the Γ point ($k_x = 0$) in the one-dimensional

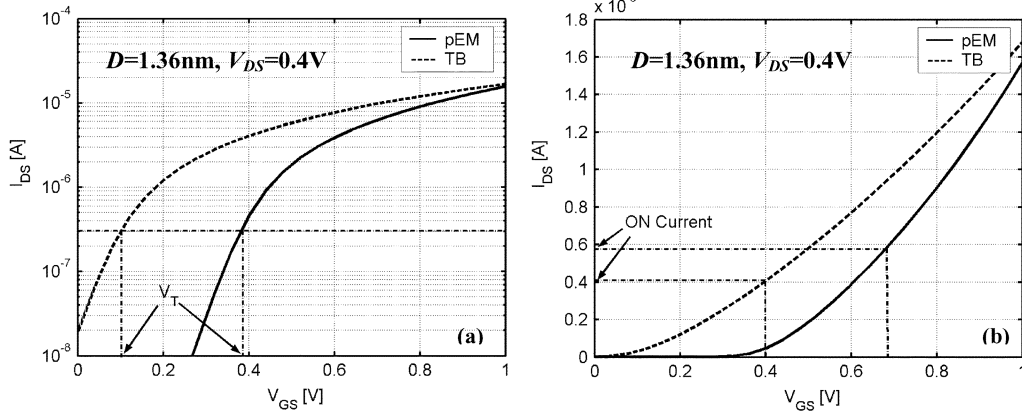


Fig. 5. I_{DS} versus V_{GS} curves for a square SNWT with $D = 1.36$ nm in both (a) a semilogarithmic scale and (b) a linear scale. The oxide thickness is 1 nm, the temperature is 300 K, and the drain bias is 0.4 V. The dashed lines are for the results based on the TB $E-k$ relations while the solid lines for the pEM results.

wire Brillouin zone ($-\pi/a_0 \leq k_x \leq \pi/a_0$) to form the conduction band edge. Two primed valleys (i.e., $[100]$ and $[\bar{1}00]$), located at $k_x = \pm 0.815 \cdot 2\pi$ in the bulk Brillouin zone, are zone-folded to $k_x = \pm 0.37\pi$ in the wire Brillouin zone to form the off- Γ states. A similar observation has been reported in [10] and [11] for square Si nanowires with a $[100]$ transport direction and four confinement directions along the equivalent $\langle 110 \rangle$ axes. In the density-of-states (DOS) versus energy plots (right column), peaks corresponding to each energy minimum (maximum) in the wire conduction (valence) band are clearly observed.

As in a Si quantum well, the degeneracy of the fourfold Γ valleys in a $[100]$ oriented square wire can be lifted by the interaction between the four equivalent valleys, which is so called “band splitting” [18]–[20]. It is clearly seen in Fig. 2 that the band splitting is more significant in the thinner wire ($D = 1.36$ nm) than in the thicker wire ($D = 5.15$ nm). Fig. 3 plots the wire width (D) dependence of the splitting energy, defined as the difference between the highest and the lowest energy (at the Γ point) of the four split conduction bands. The splitting energy is seen to fluctuate as a function of the number of atomic layers and the envelope decreases with the wire width according to D^{-3} , analogous with the band splitting observed in Si quantum wells [18]–[20].

III. VALIDITY OF THE PARABOLIC EFFECTIVE-MASS APPROACH

In this section, we adopt a seminumerical ballistic FET model to calculate the $I-V$ characteristics of n-type SNWTs based on both TB $E-k$ relations and parabolic energy bands. The main features of the ballistic FET model are illustrated in Fig. 4. Three capacitors C_G , C_S , and C_D are employed to describe the electrostatic couplings between the top of the barrier and the gate, source, and drain terminals, respectively. The potential at the top of the barrier is obtained as

$$U_{scf} = \left(\frac{C_G}{C_G + C_D + C_S} \right) V_G + \left(\frac{C_D}{C_G + C_D + C_S} \right) V_D + \left(\frac{C_S}{C_G + C_D + C_S} \right) V_S + \frac{Q_{Top}}{(C_G + C_D + C_S)} \quad (1)$$

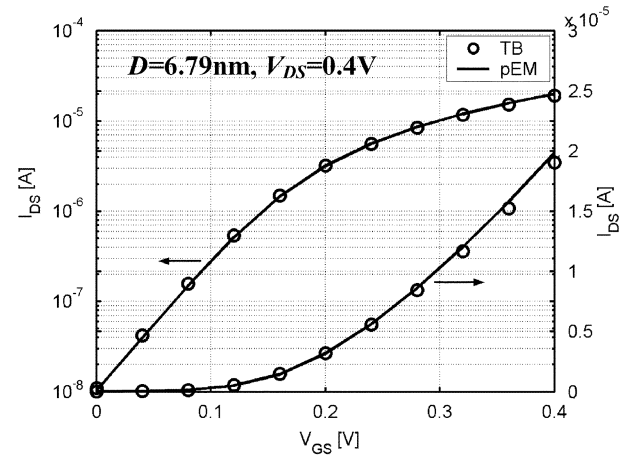


Fig. 6. I_{DS} versus V_{GS} curves for a square SNWT with $D = 6.79$ nm in both (left) semilogarithmic scale and (right) linear scale. The oxide thickness is 1 nm, the temperature is 300 K, and the drain bias is 0.4 V. The circles are for the results based on the TB $E-k$ relations while the solid lines for the pEM results.

where V_G , V_S , and V_D are the applied biases at the gate, the source, and the drain, respectively, and Q_{Top} is the mobile charge at the top of the barrier, which is determined by U_{scf} , the source and drain Fermi levels (E_{FS} and E_{FD}) and the $E-k$ relation for the channel material. To be specific, the group velocity of each state is calculated from the tabulated $E-k$ data of the nanowire, and the carrier density is then evaluated by assuming that the states with a positive (negative) group velocity are in equilibrium with the source (drain) reservoir. After self-consistency between U_{scf} and Q_{Top} is achieved, the drain current is readily obtained from the known populations of all the states in the energy bands of the wire. In previous paper, this model was used to evaluate the $I-V$ characteristics of ballistic Si MOSFETs [13] and HEMTs [14] with parabolic energy bands and Ge MOSFETs with numerical $E-k$ relations [15]. A detailed description of the model can be found in [13] and the Matlab scripts of this model are available [21].

Fig. 5 plots the I_{DS} versus V_{GS} curves for a square SNWT with $D = 1.36$ nm in both (a) a semilogarithmic scale and (b) a linear scale. The dashed lines are for the results based on the TB $E-k$ relations while the solid lines are for the parabolic effective-mass (pEM) results. In the parabolic effective-mass approach, all six conduction-band valleys in bulk Si are considered, and

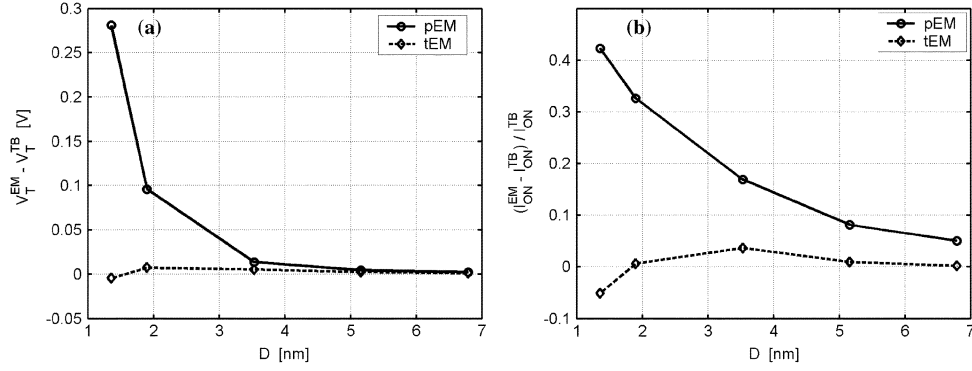


Fig. 7. Wire width dependence (D) of the errors, $V_T^{EM} - V_T^{TB}$ in (a) and $(I_{ON}^{EM} - I_{ON}^{TB})/I_{ON}^{TB}$ in (b), associated with the effective-mass approximations. The solid lines with circles are for the pEM approximation while the dashed lines with diamonds are for the tEM approach.

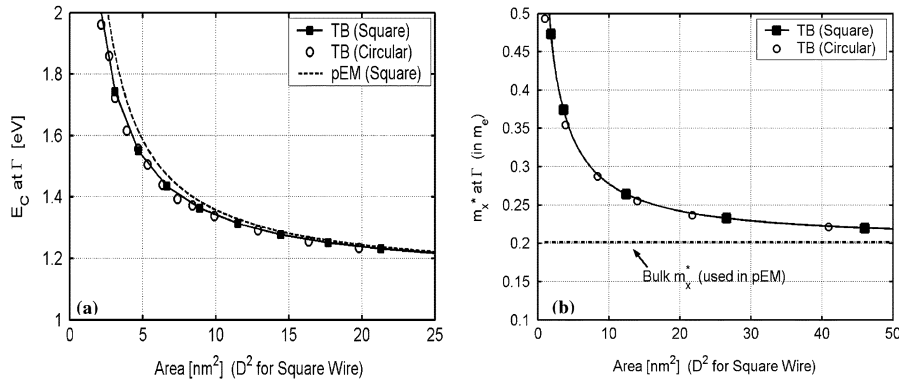


Fig. 8. (a) Conduction band edges E_C for the simulated wires with different wire widths. The solid line with squares is for the values for the square wires obtained from the TB $E-k$ relations and the dashed line is for the corresponding pEM results. For comparison, the TB values for the circular wires with a [100] wire orientation are also shown (circles). (b) The wire width (D) dependence of the transport effective-mass, m_x^* , at the Γ point in the wire conduction band (extracted from the TB energy bands by $m_x^* = \hbar^2 / (\partial^2 E / \partial^2 k_x)$, where \hbar is the Plank constant). The solid line with squares is for the square wires while circles are for the circular wires. For comparison, the bulk value of m_x^* for the unprimed valleys (used in pEM) is shown by the dash-dot line.

the effective-masses used in the calculation ($m_l = 0.891m_e$ and $m_t = 0.201m_e$) are extracted from the bulk $E-k$ relation evaluated by our TB approach with the parameters obtained from [9]. (By doing this, the $\sim 5\%$ deviation in bulk Si effective-masses caused by the TB parameters [9] are prevented from affecting our comparison between TB and pEM.) If we define a threshold voltage V_T as

$$I_{DS}(V_{GS} = V_T, V_{DS} = 0.4 \text{ V}) = 300 \text{ nA} \quad (2)$$

and an ON-current of SNWTs as

$$I_{ON} = I_{DS}(V_{GS} - V_T = 0.3 \text{ V}, V_{DS} = 0.4 \text{ V}) \quad (3)$$

we find that pEM significantly overestimates the threshold voltage by $V_T^{\text{pEM}} - V_T^{\text{TB}} = 0.28 \text{ V}$ and the ON-current by $(I_{ON}^{\text{pEM}} - I_{ON}^{\text{TB}})/I_{ON}^{\text{TB}} = 42\%$ as compared with the TB results. Fig. 6 compares pEM (solid) versus TB (circles) for the $I-V$ calculation of a thicker SNWT with $D = 6.79 \text{ nm}$. It is clear that pEM provides nearly identical $I-V$ characteristics as TB except for a small overestimation of ON-current by $\sim 5\%$. The solid lines with circles in Fig. 7 show the wire width (D) dependence of the errors, $V_T^{\text{EM}} - V_T^{\text{TB}}$ in (a) and $(I_{ON}^{\text{EM}} - I_{ON}^{\text{TB}})/I_{ON}^{\text{TB}}$ in (b), associated with pEM. It is clear that pEM starts to overestimate threshold voltage by >0.03

V when D scales below 3 nm and ON-current by $\geq 10\%$ when D is $\leq 5 \text{ nm}$.

To understand the above observations, we plot the D dependence of the wire conduction band-edges E_C and the transport effective-mass m_x^* at the Γ point in the wire conduction band (Fig. 8). (Note that the square wires are the nominal structures we focus on in this paper. For comparison, we also show the results for circular wires with the same ([100]) wire orientation. The results illustrate that the energy dispersion relations are nearly invariant when the cross-sectional shape changes from square to circular, indicating that the conclusions in this paper also apply to wires with a circular cross section.) As we can see in Fig. 8(a), when $D > 4 \text{ nm}$ (area $> 16 \text{ nm}^2$), the E_C obtained from the TB calculations (solid with squares) is well reproduced by pEM (dashed). (In pEM, the wire conduction band-edge is determined by the lowest subband level of the four unprimed valleys). At smaller wire widths, however, pEM overestimates E_C due to the nonparabolicity [22]–[25] of the bulk Si bands. This overestimation of E_C by pEM directly leads to the overvalued threshold voltages of the simulated SNWTs. The solid line with squares in Fig. 8(b) shows an increasing m_x^* (extracted from the TB $E-k$ relations) with a decreasing D , which is also a result of the nonparabolicity of the bulk Si $E-k$ relations. When $D < 3 \text{ nm}$ (Area $< 9 \text{ nm}^2$), m_x^* extracted from TB is $>40\%$ larger than the corresponding bulk value used in pEM. Since the electron thermal velocity is inversely proportional to the square

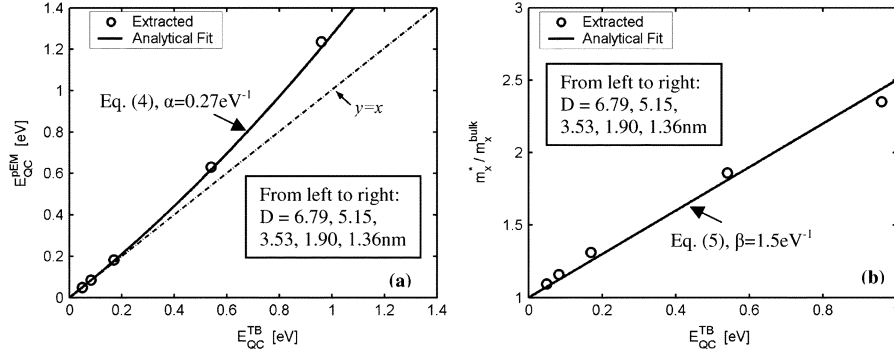


Fig. 9. (a) Quantum confinement energy computed by parabolic effective-mass (E_{QC}^{pEM}) versus that obtained from the TB calculation (E_{QC}^{TB}). (b) The ratio of the transport effective-mass, m_x^* to the bulk value, m_x^{bulk} versus the quantum confinement energy calculated by the TB approach (E_{QC}^{TB}). In both plots, the circles are for the data points extracted from the TB and parabolic $E-k$ relations, and the corresponding wire width for each point from left to right is $D = 6.79, 5.15, 3.53, 1.90, 1.36 \text{ nm}$, respectively. The solid lines are for the analytical fit based on (4) and (5).

root of the transport effective mass, the pEM calculations, which adopt a smaller m_x^* than the TB approach, overestimate the carrier injection velocity and consequently the SNWT ON-currents. In short, the nonparabolicity of the bulk Si bands plays an important role when quantum confinement is strong (small D). The use of parabolic energy bands overestimates the wire conduction band-edge and underestimates the transport effective-mass, and consequently provides a higher SNWT threshold voltage and ON-current as compared with the TB approach.

Although we have shown that the pEM approach does not perform well at small wire widths, it is still interesting to know whether it is possible to modify the effective-mass approach to obtain a better agreement with the TB calculation, since the effective-mass approximation significantly reduces computation time as compared to atomistic treatments. To do this, we first define a quantum confinement energy as the difference between the wire conduction band-edge, E_C and that for bulk Si ($E_C^{\text{bulk}} = 1.13 \text{ eV}$). Fig. 9(a) shows the quantum confinement energy computed by pEM (E_{QC}^{pEM}) versus that obtained from the TB calculation (E_{QC}^{TB}). It is evident that for small wire widths, the data points (circles) stand above the $y = x$ curve, indicating that pEM overestimates the quantum confinement energy when it is large. Inspired by the expressions for the nonparabolicity of the bulk Si bands [22], [23], we propose the following quadratic equation to analytically describe the E_{QC}^{pEM} versus E_{QC}^{TB} relation

$$E_{QC}^{TB} \cdot (1 + \alpha \cdot E_{QC}^{TB}) = E_{QC}^{pEM} \quad (4)$$

where α is treated as a fitting parameter and $\alpha = 0.27 \text{ eV}^{-1}$ is used for the solid line in Fig. 9(a) for the best agreement with the extracted data. Similarly, the E_{QC}^{TB} dependence of the transport effective-mass m_x^* at the Γ point [Fig. 9(b)] can also be described by the following equation:

$$m_x^* = m_{\text{bulk}}^* (1 + \beta \cdot E_{QC}^{TB}) \quad (5)$$

where $m_{\text{bulk}}^* = m_t = 0.201 m_e$ is the transport effective-mass in the unprimed valleys in bulk Si and $\beta = 1.5 \text{ eV}^{-1}$ is chosen to achieve the best match between the extracted data points (circles) and the analytical expression (solid) up to $E_{QC}^{TB} = 1 \text{ eV}$, which is sufficient for the $I-V$ calculation of the simulated Si nanowire transistors.

After knowing (4) and (5), the effective-mass approximation can be tuned for a better fit with TB in the following steps.

- Step 1) Calculate the quantum confinement energy, E_{QC}^{pEM} by the parabolic effective-mass approach with the bulk effective-masses (i.e., m_y^* and m_z^*).
- Step 2) Solve (4) to obtain the updated quantum confinement energy E_{QC}^{new} as

$$E_{QC}^{\text{new}} = \frac{-1 + \sqrt{1 + 4\alpha \cdot E_{QC}^{pEM}}}{2\alpha}. \quad (6)$$

- Step 3) Evaluate the tuned transport effective-mass at the Γ point by (5),

$$m_x^* = m_{\text{bulk}}^* (1 + \beta \cdot E_{QC}^{\text{new}}). \quad (7)$$

- Step 4) Use the computed E_{QC}^{new} and m_x^* for the $I-V$ calculation of SNWTs.

It should be noted that the above tuning process is only necessary for the four unprimed valleys because: 1) at large wire widths, the quantum confinement energy is small and nonparabolicity is insignificant in both unprimed and primed valleys, so the parabolic effective-mass approach performs well and 2) at small wire widths, the two primed valleys are well separated from the unprimed ones due to stronger quantum confinement (smaller effective-masses in the y and z directions) in these primed valleys, so the electron density and current contributed by the primed valleys are negligible (e.g., when $E_{QC}^{TB} > 0.15 \text{ eV}$, over 97% electrons are distributed in the unprimed valleys).

The dashed lines with diamonds in Fig. 7 show the wire width (D) dependence of the errors, $V_T^{\text{EM}} - V_T^{\text{TB}}$ in (a) and $(I_{\text{ON}}^{\text{EM}} - I_{\text{ON}}^{\text{TB}})/I_{\text{ON}}^{\text{TB}}$ in (b), associated with the *tuned* effective-mass approximation. For wire widths ranging from 1.36 to 6.79 nm, the tuned effective-mass approach provides an excellent match with the TB calculation—less than 10-mV error for V_T and less than 5% error for I_{ON} . So far, we have shown that the effective-mass approximation can be modified by introducing two D -independent parameters, α and β , to accurately reproduce the $I-V$ results computed by TB. It must be mentioned that the *values* of α and β used in this paper were obtained for SNWTs with one particular channel orientation (i.e., [100]) and one specific cross-sectional shape (i.e., square

with all faces along the equivalent $\langle 100 \rangle$ axes). The important point is that for I - V calculation it is possible to simply tune the effective-mass approach to fit the TB model. We expect that this conclusion may apply to other SNWTs with different transport directions and cross sections while the values of the tuning parameters (α and β) are subject to change.

IV. CONCLUSION

By using an $sp^3d^5s^*$ TB approach as a benchmark, we examined the validity of the parabolic effective-mass approximation for the I - V calculation of n-type silicon nanowire transistors. It was found that the simple parabolic effective-mass approach with bulk effective-masses significantly overestimates SNWT threshold voltages when the wire width (D) is <3 nm, and ON-currents when $D < 5$ nm. However, by introducing two analytical equations with two tuning parameters, the effective-mass approximation can well reproduce the TB I - V results over a wide range of wire widths—even at $D = 1.36$ nm. In conclusion, bandstructure effects begin to manifest themselves in silicon nanowires with small diameters, but with a simple tuning procedure, the parabolic effective-mass approximation may still be used to assess of the performance limits of silicon nanowire transistors.

ACKNOWLEDGMENT

The authors wish to thank Prof. S. Datta at Purdue University for fruitful discussions.

REFERENCES

- [1] Y. Taur and T. H. Ning, *Fundamentals of Modern VLSI Devices*. Cambridge, U.K.: Cambridge Univ. Press, 1998.
- [2] Y. Cui, Z. Zhong, D. Wang, W. Wang, and C. M. Lieber, "High performance silicon nanowire field effect transistors," *Nano. Lett.*, vol. 3, no. 2, pp. 149–152, Feb. 2003.
- [3] F.-L. Yang *et al.*, "5 nm gate nanowire FET," in *Symp. VLSI Tech. Dig.*, Jun. 2004, pp. 196–197.
- [4] B. S. Doyle *et al.*, "High performance fully-depleted tri-gate CMOS transistors," *IEEE Electron Device Lett.*, vol. 24, no. 4, pp. 263–265, Apr. 2003.
- [5] H. Majima, Y. Saito, and T. Hiramoto, "Impact of quantum mechanical effects on design of nano-scale narrow channel n- and p-type MOSFETs," in *IEDM Tech. Dig.*, Dec. 3–5, 2001, pp. 951–954.
- [6] J. Wang, E. Polizzi, and M. Lundstrom, "A three-dimensional quantum simulation of silicon nanowire transistors with the effective-mass approximation," *J. Appl. Phys.*, vol. 96, no. 4, pp. 2192–2203, Aug. 2004.
- [7] ———, "A computational study of ballistic silicon nanowire transistors," in *IEDM Tech. Dig.*, Dec. 8–10, 2003, pp. 695–698.
- [8] H. Takeda and N. Mori, "Three-dimensional quantum transport simulation of ultra-small FinFETs," in *Proc. 10th Int. Workshop Computational Electronics (IWCE-10)*, sec. 8-04, Oct. 25–27, 2004.
- [9] T. B. Boykin, G. Klimeck, and F. Oyafuso, "Valence band effective-mass expressions in the $sp^3d^5s^*$ empirical tight-binding model applied to a Si and Ge parametrization," *Phys. Rev. B, Condens. Matter*, vol. 69, Mar. 2004.
- [10] Y. J. Ko, M. Shin, S. Lee, and K. W. Park, "Effects of atomic defects on coherent electron transmission in Si nanowires: Full band calculations," *J. App. Phys.*, vol. 89, no. 1, pp. 374–379, Jan. 2001.
- [11] Y. Zheng, C. Rivas, R. Lake, K. Alam, T. B. Boykin, and G. Klimeck, "Electronic properties of silicon nanowires," *IEEE Trans. Electron Devices*, vol. 52, no. 6, pp. 1097–1103, Jun. 2005.
- [12] J. Wang, A. Rahman, A. Ghosh, G. Klimeck, and M. Lundstrom, "Performance evaluation of silicon nanowire transistors with atomic-basis dispersion relations," *Appl. Phys. Lett.*, vol. 86, Feb. 2005. Art. no. 093 113.
- [13] A. Rahman, J. Guo, S. Datta, and M. Lundstrom, "Theory of ballistic nanotransistors," *IEEE Trans. Electron Devices*, vol. 50, no. 9, pp. 1853–1864, Sep. 2003.
- [14] J. Wang and M. Lundstrom, "Ballistic transport in high electron mobility transistors," *IEEE Trans. Electron Devices*, vol. 50, no. 7, pp. 1604–1609, Jul. 2003.
- [15] A. Rahman, G. Klimeck, and M. Lundstrom, "Bandstructure effects in ballistic nanoscale MOSFETs," in *IEDM Tech. Dig.*, 2004, pp. 139–140.
- [16] X. Zhao, C. Wei, L. Yang, and M. Y. Chou, "Quantum confinement and electronic properties of silicon nanowires," *Phys. Rev. Lett.*, vol. 92, no. 23, Jun. 2004. Art. no. 236 805.
- [17] S. Lee, F. Oyafuso, P. von Allmen, and G. Klimeck, "Boundary conditions for the electronic structure of finite-extent embedded semiconductor nanostructures," *Phys. Rev. B, Condens. Matter*, vol. 69, Jan. 2004.
- [18] T. B. Boykin *et al.*, "Valley spitting in strained silicon quantum wells," *App. Phys. Lett.*, vol. 84, no. 1, pp. 115–117, Jan. 2004.
- [19] A. Rahman, G. Klimeck, M. Lundstrom, N. Vagidov, and T. B. Boykin, "Atomistic approach for nano-scale devices at the scaling limit and beyond—Valley splitting in Si," *Jpn. J. Appl. Phys.*, no. 4B, p. 2187, Apr. 2004.
- [20] T. B. Boykin, G. Klimeck, M. Friesen, S. N. Coppersmith, P. von Allmen, F. Oyafuso, and S. Lee, "Valley splitting in low-density quantum-confined heterostructures studied using tight-binding models," *Phys. Rev. B, Condens. Matter*, vol. 70, Oct. 2004. Art. no. 165 325.
- [21] NanoHUB [Online]. Available: <http://nanohub.org>
- [22] M. Lundstrom, *Fundamentals of Carrier Transport*, Cambridge, U.K.: Cambridge Univ. Press, 2000.
- [23] L. Reggiani, *Hot Electron Transport in Semiconductors*. New York: Springer-Verlag, 1985.
- [24] S. Tomic, E. P. O'Reilly, P. J. Klar, H. Gruning, W. Heimbrodt, W. Chen, and I. A. Buyanova, "Influence of conduction-band nonparabolicity on electron confinement and effective mass in $\text{GaN}_x\text{As}_{1-x}/\text{GaAs}$ quantum wells," *Phys. Rev. B, Condens. Matter*, vol. 69, no. 24, Jun. 2004. Art. no. 245 305.
- [25] W. Wang, T. Hwang, W. Lin, and J. Liu, "Numerical methods for semiconductor heterostructures with band nonparabolicity," *J. Comput. Phys.*, vol. 190, no. 1, pp. 141–158, Sep. 2003.



Jing Wang (S'03) was born in China in 1979. He received the B.E. degree from the Department of Electronic Engineering, Tsinghua University, Beijing, China, in 2001. He is currently pursuing the Ph.D. degree at the School of Electrical and Computer Engineering, Purdue University, West Lafayette, IN.

His research interests center on the theory and simulation of nanometer scale electronic devices, which includes the modeling and design of nanoscale MOSFETs and post-CMOS transistors, as well as

the transport theory for HEMTs.

Mr. Wang is a student member of the American Physical Society (APS).



Anisur Rahman received the B.Sc. degree in electrical and electronics engineering from the Bangladesh University of Engineering and Technology, Dhaka, Bangladesh, in 1997. He is currently pursuing the Ph.D. degree at the Purdue Nanotransistor Research Group, Purdue University, West Lafayette, IN.

In the Fall of 1999, Purdue Nanotransistor Research Group, Purdue University. His research interests are centered around the physics of decananometer-scale MOSFET devices and includes their designing, analytical modeling, and prospect of performance enhancement through the use of novel-channel materials.

Avik Ghosh received the M.S. degree in physics from the Indian Institute of Technology, Kanpur, India, in 1994, and the Ph.D. degree in physics from The Ohio State University, Columbus, in 1999.

He then joined Purdue University, West Lafayette, IN, as a Postdoctoral Research Fellow in electrical engineering, and is now a Research Scientist at Purdue University, where he works on electron transport in nanoscale devices, including atomic and molecular wires, nanoscale silicon MOSFETs, hybrid silicon molecular devices, quantum dots, and carbon nanotubes. Among his other research activities are ultrafast optical phenomena in semiconductor heterostructures and noise-induced transport in Brownian environments.



Gerhard Klimeck (M'95) received the degree in electrical engineering from Ruhr-University Bochum, Germany, in 1990, and the Ph.D. degree from Purdue University, West Lafayette, IN, in 1994.

He is the Technical Director of the Network for Computational Nanotechnology at Purdue University and a Professor of Electrical and Computer Engineering since 2003. He leads the development and deployment of web-based simulation tools that are hosted on <http://nanohub.org>, a community website utilized by over 5000 users annually. He was the

Technical Group Supervisor for the Applied Cluster Computing Technologies Group and continues to hold his appointment as a Principal Member at the Jet Propulsion Laboratory, California Institute of Technology, on a faculty part-time basis. His research interest is in the modeling of nanoelectronic devices, parallel cluster computing, genetic algorithms, and parallel image processing. He has been the lead on the development of NEMO 3-D, a tool that enables the simulation of multimillion atom quantum dot systems, and NEMO 1-D, the first nanoelectronic CAD tool. Previously, he was a Member of Technical Staff at the Central Research Laboratory, Texas Instruments, Dallas, TX. His work is documented in over 120 peer-reviewed publications and over 190 conference presentations.

Dr. Klimeck is a member of APS, HKN, and TBP.



Mark Lundstrom (F'94) received the B.E.E. and M.S.E.E. degrees from the University of Minnesota, Minneapolis, in 1973 and 1974, respectively, and the Ph.D. degree from Purdue University, West Lafayette, IN, in 1980.

He is the Scifres Distinguished Professor of Electrical and Computer Engineering at Purdue University, where he also directs the National Science Foundation's Network for Computational Nanotechnology. Before attending Purdue, he was with Hewlett-Packard Corporation, Loveland, CO,

working on integrated circuit process development and manufacturing. His current research interests center on the physics of semiconductor devices, especially nanoscale transistors. His previous work includes studies of heterostructure devices, solar cells, heterojunction bipolar transistors, and semiconductor lasers. During the course of his career at Purdue, he has served as Director of the Optoelectronics Research Center and Assistant Dean of the Schools of Engineering.

Dr. Lundstrom is a Fellow of the American Physical Society and the recipient of several awards for teaching and research—most recently the 2002 IEEE Cleo Brunetti Award and the 2002 Semiconductor Research Corporation Technical Achievement Award for his work with S. Datta on nanoscale electronics.